

F. T. ULABY

C. DOBSON

J. STILES

R. K. MOORE

J. HOLTZMAN

Remote Sensing Laboratory

University of Kansas Center for Research, Inc.

Lawrence, KS 66045

A Simulation Study of Soil Moisture Estimation by a Space SAR

It appears that a spatial resolution between 100 m and 1 km would provide optimum performance over the various soil moisture conditions considered.

INTRODUCTION

SEVERAL INVESTIGATIONS have been conducted over the past decade to evaluate the capabilities of radar as a soil moisture sensor.¹⁻¹² Through the use of ground-based and airborne scatter-

fields. Analyses of individual scene parameters and of combinations of parameters have led to the following conclusions:

- For monitoring soil moisture content in non-irrigated regions, the optimum sensor parameters

ABSTRACT: *Image simulation techniques were employed to generate synthetic aperture radar (SAR) images of a 17.7 km by 19.3 km test site located east of Lawrence, Kansas. The simulations were performed for a space SAR at an orbital altitude of 600 km with the following sensor parameters: frequency = 4.75 GHz, polarization = HH, and angle of incidence range = 7° to 22° from nadir. Three sets of images were produced corresponding to three different spatial resolutions: 20 m by 20 m with 12 looks, 100 m by 100 m with 23 looks, and 1 km by 1 km with 1000 looks. Each set consisted of images for four different soil moisture distributions across the test site. The purpose of this study was to evaluate the accuracy with which soil moisture could be predicted for each of the 12 resolution/soil moisture distribution combinations. The input information used to specify the gray level of each of the 800,000 pixels contained in the image included (when applicable) soil moisture, soil type, vegetation cover, surface roughness, row direction (relative to the radar look direction), and local slope. The prediction algorithm is based on a generalized formula relating the received power to soil moisture, with no information available to it on the scene properties except for the angle of incidence with respect to the mean elevation of the test site. The results indicate that, for the agricultural portion of the test site, the soil moisture of about 90 percent of the 20 m by 20 m pixels can be predicted with an accuracy of ± 20 percent of field capacity. Among the three spatial resolutions, the 1 km by 1 km resolution gave the best results for most cases; however, for very dry soil conditions, the 100 m by 100 m resolution was slightly superior.*

ometers, these investigations examined the dependence of the radar backscattering coefficient, σ° , on soil moisture content, surface roughness, vegetation cover, soil type (texture), and row direction (relative to radar look direction) of tilled

are f in the 4 to 5 GHz range, θ in the 7° to 22° range, and a polarization configuration of HH (or HV). Optimality is defined in terms of minimum error in predicting soil moisture without *a priori* knowledge of soil surface roughness and surface cover (whether vegetation is present or not).

- For monitoring soil moisture content in irrigated regions where tillage practices are used, the above sensor configuration is still applicable provided HV polarization is used. The choice of HV polarization is based on experimental observations that have shown that the cross-polarized scattering coefficient is significantly less sensitive to row direction than is the like-polarized scattering coefficient.
- The σ^0 response to gravimetric (or volumetric) soil moisture content is dependent upon soil type, but the response to the moisture content when referenced to the 1/3 bar moisture content (which sometimes is defined as the field capacity) is approximately independent of soil type.
- The depth layer of the soil where the radar responds to soil moisture appears to vary between about 1 cm for very wet conditions to about 15 cm for dry soil; overall, the moisture in the 0 to 5 cm surface layer appears to adequately describe the response.

The present study was an attempt to evaluate the accuracy of the soil moisture estimate that a spaceborne radar imager could provide. An additional objective of this study was to evaluate the influence of spatial resolution on the estimation accuracy. These evaluations were accomplished through the use of image simulation techniques. "Realistic" radar images, generated by incorporating all known effects of scene properties and sensor operational characteristics, provide a useful means of evaluating the *integrated* effects of many scene parameters on the radar response to soil moisture. Of course, results based on "simulations" are inherently limited by the validity of the input information used in the simulation. Hence, special care was taken to insure that models used for characterizing the backscatter behavior were adequately supportable by experimental evidence.¹³

SYSTEM CONFIGURATION

Imaging radars for soil moisture determination may take on several different configurations depending upon the resolution needed. A major purpose of this study was to determine the required resolution and, consequently, its impact on radar system parameter selection.

Should fine resolutions be required, no alternative exists to the nearly fully-focused synthetic aperture radar (SAR). On the other hand, as the required resolution becomes coarser, the options available to the system designer increase. Various forms of partially-focused and unfocused SAR may be used. When the resolution requirement is coarse enough, one may consider using a real-aperture sidelooking radar (RAR). A "RAR" is much easier to build than a "SAR," so that this option must be examined seriously. Furthermore, when the resolution requirement is relatively modest, one may consider a combined microwave radiometer and scanning synthetic aperture radar

(RADISAR). The resolution for the radar system can be of the order of hundreds of metres, whereas that for the radiometer will be a few kilometres or tens of kilometres, but the SAR picture is embedded within the radiometer cell so that the two may be used jointly for the soil-moisture determination.

As the radar resolution requirement is tightened, the required power, data rate, and processing complexity increase. The power required for the RAR is usually quite small with the swath-width that one used for soil-moisture determination. The power required for a partially-focused or unfocused SAR may also be quite small under these conditions. The power for the RADISAR may be extremely small because the total antenna area may be larger for a RADISAR than for a sidelooking radar that does not scan its beam.

The complexity of the processing for fine-resolution SAR precludes on-board processing. However, for coarser resolution SAR, the complexity is reduced to such an extent that one may think very seriously about on-board processing, which in turn reduces the required telemetry rate to an almost negligible level. Therefore, one must examine the resolution requirement very carefully and determine from this whether the advantages of fine resolution for other purposes should be traded for the advantages of coarse resolution in terms of low power, onboard processing, and low telemetry rate.

The spacecraft configuration considered in this study is given in Table 1. From the fundamental geometric parameters, one can calculate certain other derived geometric parameters as shown in Figure 1, which include ground swath-width (143 km) and slant swath-width (38.5 km). These parameters are common to all of the systems considered here, the primary variables being ground resolution in both across-track direction r_y and along-track direction r_a . The number of independent samples averaged (number of independent looks) N is a very important factor that must be considered in evaluating the performance of a system of this kind. For a given set of values of r_y , r_a , and N , it is possible to compute an approximate equivalent spatial resolution r_e of a square pixel of photographic quality (no speckle) having equivalent interpretability.¹⁴

Various system configurations have been postulated for soil moisture determination, with the reference system being a fully-focused SAR with an antenna 8.7 m long and with a square pixel at $\theta = 7^\circ$. Table 2 summarizes some of the characteristics of the systems considered, which include r_a by r_y at $\theta = 7^\circ$ and at $\theta = 22^\circ$, the equivalent resolution r_e at each end of the angular range for the number of looks (N) used, and the average transmitter power required. Details of the computations that led to the values given in Table 2 are available in Ulaby *et al.*¹³

The simulated images generated in this study

TABLE 1. SPACECRAFT RADAR CONFIGURATION

Spacecraft Height	h	600 km
Radar Frequency	f	4.75 GHz
Angle of Incidence Range	θ	$7^\circ - 22^\circ$
Antenna Pointing Angle Range	δ	$6.39^\circ - 20.02^\circ$ (curved Earth)
Receiver Noise Figure	F	4 (6 dB)
Minimum Signal-to-Noise Ratio	S_n	4 (6 dB)
System Loss Allowance		2 (3 dB)
Minimum Scattering Coefficient	σ_{\min}°	-21 dB
Antenna Length	D	8.7 m (8.7 m and 15 m for RAR and 5 m for RADISAR)
Antenna Radiation Efficiency	η	0.75
Ground Swath-Width	S_g	143 km
Slant Swath-Width	R_a	38.5 km

are of a test site, 17.7 km by 19.3 km in size, located east of Lawrence, Kansas. As will be discussed later, the data base used for simulating a radar image consisted of approximately 800,000 pixels, 20 m by 20 m each. Thus, simulating the entire ground swath-width (143 km) in a single image would have required a large and cumbersome data base. Therefore, it was decided to use the available test site to simulate images corresponding to a select set of narrow angular ranges across the radar elevation beamwidth. These sets, each 2° to 3° wide, were performed at the mid-angles of 8.2° , 12.1° , and 19.8° . Also, not all of the examples illustrated in Table 2 could be simulated; the simulation process is an expensive and time-consuming one, and the simulations must start with a spatial resolution comparable to that of the data base, which is 20 m by 20 m. For this reason, the simulations were performed for only three configurations. These configurations are not identical to those in Table 2, but very close to cases 2, 4, and 8, as indicated in Table 3. Although, for a given configuration (case), the azimuth and range resolutions, r_a and r_r , are not always equal, for ease of reference, the three simulated configurations shall henceforth be referred to as the 20 m, 100 m, and 1 km resolutions.

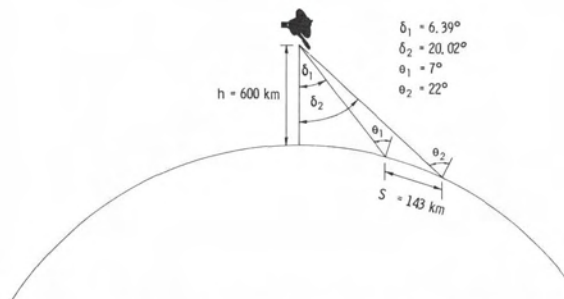


FIG. 1. Side-looking SAR observing a curved earth from an altitude of 600 km.

DATA BASES

The test site used consisted of 800,000 pixels, 20 m by 20 m each in size. Prior to generating a radar image, the following data bases were constructed:

LAND USE

Target class data were extracted from a U-2 color IR photograph of the test site. The image was divided into four quadrants and each quadrant was digitized into a 512 by 512 matrix on a CRT by use of a video camera. Manual interpretation of the U-2 imagery, augmented by low-altitude USDA/SCS imagery, allowed assignment of a target land-use class to each of the 512 by 512 pixel elements on each quadrant. A list of target categories used to characterize land use within the data base is given in Table 4, and Figure 2 shows the resultant land use map.

SOIL TEXTURAL CLASSIFICATION

A digital matrix of soil textural class was constructed for all 20 m by 20 m pixel elements in the data base using USDA/SCS county soil surveys as data sources. Each pixel element was classified as belonging to one of ten different soil textural classes or complexes. Figure 3 shows the digitized soil textural overlay for the test site. Each soil textural class was assumed to have characteristic sand, silt, and clay components as given in Table 5. These textural components were then used to determine a characteristic 1/3-bar water content for each soil textural class with an empirical expression from Schumge.¹⁵

SURFACE ELEVATION

The distribution of surface elevation above mean sea level was encoded into the data base using USGS 7.5 minute series topographic maps. Figure 4 gives a shaded relief presentation of the elevation matrix.

DATA BASE REGISTRATION

The initial digital data base consisted of separate matrices for target class, soil texture, and sur-

TABLE 2. POTENTIAL SYSTEM DESIGN OPTIONS

Case Type #		Slant Range Resolution r_R (m)	Number of Looks Available in Azimuth	Number of Looks Used N	7°		22°		Average Power (W)
					$r_a \times r_b$ (m × m)	Equiv. Square Photo Pixel (m × m)	$r_a \times r_b$ (m × m)	Equiv. Square Photo Pixel (m × m)	
1	Fully-focused SAR	0.52	1	1	4.1 × 4.3	19.6 × 19.6	4.4 × 1.4	11.6 × 11.6	9850
2	Partially-focused SAR	3.75	2.3	12	9.3 × 31	25 × 25	10 × 10	14.7 × 14.7	7198
3	Partially-focused SAR	11.2	6.9	12	28 × 92	75 × 75	30 × 30	44 × 44	800
4	Partially-focused SAR	11.2	23	23	93 × 92	122 × 122	100 × 30	72 × 72	460
5	Partially-focused SAR	37.5	23	23	93 × 307	223 × 223	100 × 100	132 × 132	138
6	Unfocused SAR	37.5	69	69	280 × 307	343 × 343	300 × 100	202 × 202	138
7	Unfocused SAR	112	69	69	280 × 922	594 × 594	300 × 300	351 × 351	46
8	Unfocused SAR	112	230	230	934 × 922	1010 × 1010	1000 × 300	596 × 596	46
8a	Unfocused SAR	375	69	69	280 × 3074	1084 × 1084	300 × 1000	640 × 640	13.8
9	RAR ($D = 8.7$ m)	26.6	1049	1049	4264 × 218	1004 × 1004	4564 × 71	592 × 592	194
10	RAR ($D = 15$ m)	45.0	363	363	2545 × 369	1036 × 1036	2724 × 120	616 × 616	38.6
11	Unfocused SAR	375	230	230	934 × 3074	1844 × 1844	1000 × 1000	1088 × 1088	13.8
12	RAR ($D = 15$ m)	375	363	363	2545 × 3074	2992 × 2992	2724 × 1000	1765 × 1765	4.6
13	RAR ($D = 8.7$ m)	562	1049	1049	4263 × 4611	4613 × 4613	4564 × 1500	2722 × 2722	9.2
14	RADISAR (5 m × 5 m antenna 19 scan positions)	213	12	12	532 × 532	785 × 785	570 × 173	463 × 463	0.66

TABLE 3. SIMULATIONS COMPARED WITH NEAREST SYSTEM CASE

Simulation Case	θ	r_a (m)	r_y (m)	N	r_e (m)	Nearest System Case	r_e at θ (m)
A1	8.2°	20	20	12	29.5	2	25 at 7°
A2	12.1°	20	20	12	29.5	2	25 at 7°
A3	19.8°	20	20	13	29.0	2	25 at 7°
B1	8.2°	90	100	23	125	4	122 at 7°
B2	12.1°	93	60	27	96	4	94 at 12°
C1	8.2°	900	1000	2250	974	8	976 at 7.5°
C2	12.1°	900	600	2800	753	8	750 at 13°

face elevation in four quadrants each. A set of 8 to 12 registration points had been preselected within each quadrant. An n th order polynomial fit to the registration points established a warping function for mapping all soil texture and surface-elevation matrices into the coordinate system of the corresponding target class matrix. This process corrected for any lack of geometric equivalence in the raw data sources and any scaling differences arising from the digitization procedure. Upon com-

pletion of the warping, all four quadrants were then mapped into a common coordinate system and aligned, and overlap data were then deleted from the composite data base.

SIMULATION OF RAINFALL AND SOIL MOISTURE DISTRIBUTIONS

In order to produce realistic simulations, four hypothetical soil moisture distributions were developed for the 0 to 5 cm soil layer. These distributions cover the full range of potential moisture conditions from saturation of the soil to a drought-like condition. With respect to time, the hypothetical moisture conditions cover a 35-day time-span with simulated satellite overpasses on days 4, 5, 15, and 35.

TABLE 4. AREA PERCENT OF TOTAL DATA BASE ASSIGNED TO EACH TARGET CLASS

Target Class	Percent of Total Area
Roads	3.76
Railroads	0.12
River Bridges	0.01
City Structures	0.85
Rivers	2.19
Lakes, Ponds, Impondments	0.48
Smooth Bare Soil (RMS height < 2 cm)	6.63
Medium Rough Bare Soil (2 cm < RMS height ≤ 4 cm)	4.92
Rough Bare Soil (RMS height > 4 cm)	2.75
Mown Pasture	7.06
Pasture	15.93
Alfalfa	4.15
Wheat	6.65
Sandbars	0.35
Deciduous Trees	13.03
Soybeans N/S Rows	5.46
Soybeans E/W Rows	5.62
Milo N/S Rows	2.76
Milo E/W Rows	2.27
Corn N/S Rows	8.32
Corn E/W Rows	6.61

2.67

11.08

5.03

14.93

SOIL MOISTURE CONDITIONS

For each satellite overpass, the "actual" moisture M_{FC_N} of each 20 m by 20 m pixel element in the data base is established from a hypothetical rainfall and evaporative history. The objective is to establish a set of moisture conditions for each radar simulation that is a reasonable facsimile of common "real world" conditions. In order to



FIG. 2. Land-use categories at the Eudora test site (11 by 12 miles).



FIG. 3. Soil classes within the test site.

simplify the calculations and also because of a lack of adequate source data, several assumptions are made. First, the hydraulic conductivities of all soil textural classes in the data base are assumed to be equivalent. The mean bulk densities of all soils are assumed to be 1.0 g/cm^3 within the 0 to 5 cm soil layer. In addition, the evaporation rates from all soils and crop classes are assumed to be equal although still time-dependent. In actuality, of course, bulk density, evaporation rate, and hydraulic conductivity all vary as functions of many variables including soil moisture, soil texture, and crop class.

For each 20 m by 20 m pixel, soil moisture M_{FC_N} is computed from the general expression

$$M_{FC_N} = M_{FC_{(N-1)}} + 100(M_{V_N}/FC_{\text{vol}}) \quad (1)$$

where

M_{FC_N} = % of 1/3-bar water content for the N th simulation;

M_{V_N} = the change in volumetric water content since the time of the $(N-1)$ simulation, g/cm^3 ; and

FC_{vol} = estimated 1/3-bar water content, g/cm^3 .

Since soil bulk density is assumed to be 1.0 g/cm^3 , then

$$FC_{\text{vol}} = 1.0 \times FC \quad (2)$$

for values of FC given in Table 5 for each soil texture. In addition, M_{V_N} is dependent upon incident rainfall, surface and subsurface drainage, and evaporation. That is,

$$M_{V_N} = M_{V_{(N-1)}} + M_{\text{rain}} - M_{\text{evap}} \quad (3)$$

where

$M_{V_{(N-1)}}$ = initial volumetric soil moisture,

M_{rain} = net increase in M_V due to precipitation, and

M_{evap} = net loss in M_V due to evaporative demand.

Since soil bulk density is assumed equal to 1.0 g/cm^3 , M_{rain} and M_{evap} can be calculated from incident rainfall and evaporation rate by

$$M_{\text{rain}} = (\text{Precipitation} - \text{Drainage}) / \text{Soil Depth} \quad (4)$$

and

$$M_{\text{evap}} = (\text{Evaporation rate} \times \text{elapsed time}) / \text{Soil Depth} \quad (5)$$

where precipitation, drainage, and soil depth are in cm and evaporation rate is in cm per day.

The simplicity of the moisture model described does not detract from its usefulness because the model serves only to vary surface moisture spatially and temporally for the radar simulations.

POSTULATED RAINFALL AND EVAPORATIVE HISTORY

During the first day of the 35-day time-span, a steady and heavy rain is assumed to have produced saturated soil moisture conditions over the entire data base. Over the next three days, water in excess of field capacity (as estimated by the water retention of a given soil at 1/3 bar) is assumed to have drained from the upper 5 cm of soil throughout the data base. Thus, a satellite overpass on day four observes all soils with M_{FC} equal to 100 percent of 1/3-bar water content.

Less than a day after the first simulated radar overpass, a hypothetical convective thunderstorm passes from west to east across the data base. The storm deposits a Gaussian rainfall distribution with maximum incident rainfall of 2.5 cm along the center of the storm-track and with a minimum approaching 0.0 cm along the northern and southern edges of the data base. Limited hydraulic conductivity of the soil causes all incident rainfall in excess of 1.25 cm to drain laterally from the soil as surface run-off. Any incident rainfall less than 1.25 cm is assumed to percolate rapidly into the upper 5 cm of soil. Thus, immediately after passage of the thunderstorm, maximum M_{rain} is 0.25 g/cm^3 from Equation 4. A satellite overpass of the data base several hours after passage of the thunderstorm could be expected to observe a soil moisture distribution similar to the one defined above for Day 5 and used in the second radar simulation.

During the following 10 days the upper 5 cm of soil dries from evaporation at a rate of 0.1 cm of water per day. There is no additional rainfall. Thus M_{evap} is a constant 0.2 g/cm^3 over the data base from Equation 5. In addition, it is assumed that for any given pixel element $M_{FC_N} \geq 25.0$ percent of 1/3-bar water content on Day 15. This assumption reflects the capacity of most soils to replenish some portion of daytime evaporative loss during the night through capillary recharge and vapor flow. A lower limit of 25 percent on surface mois-

TABLE 5. SOIL TEXTURAL CLASSES, THEIR AREA PERCENT, AND CHARACTERISTIC 1/3-BAR WATER CONTENTS WITHIN THE SIMULATION DATA BASE

Soil Textural Class	Textural Components			1/3-Bar Water Content* FC	Percent Area of Total Data Base
	% Sand	% Silt	% Clay		
Sand	92	5	3	0.0644	0.1
Loamy sand	82	13	5	0.0898	5.5
Sandy loam	65	25	10	0.1365	4.3
Loam	40	40	20	0.2110	18.0
Silt loam	20	65	15	0.2420	35.4
Silty clay loam	10	57	33	0.3076	13.1
Silty clay	7	47	46	0.3375	3.3
Clay loam	33	34	33	0.2453	13.0
Complex (50% loam and 50% silty clay loam)	25	48.5	26.5	0.2568	0.7
Complex (50% silt loam and 50% silty clay loam)	15	61	24	0.2723	6.6

* 1/3-bar water content is expressed as a weight percent of dry soil.

ture also functions to prevent unnaturally dry moisture conditions in the simulation, which otherwise could approach "oven dryness" at 0 percent M_{FC} for sandy soils in the data base which have small volumetric water retentions at 1/3 bar. Thus, a simulated radar overpass on Day 15 observes soil moisture conditions with a maximum M_{FC} of approximately 90 percent and a minimum set at 25 percent.

From the third simulation until the end of the 35-day period there is no additional precipitation, hence M_{rain} equals 0.0 g/cm³. Because at low surface-moisture conditions evaporative rate is limited by the availability of near-surface water, the evaporation rate for this 20-day period is assumed to be reduced to 0.05 cm of water per day.

As a result, M_{evap} in Equation 5 becomes 0.2 g/cm³. In order to prevent M_{FC} of sandy soils from becoming zero, a lower limit of $M_{FC} = 10$ percent is assumed to be valid on Day 35. Moisture conditions of 10 percent of 1/3-bar water retention approximates the hygroscopic coefficient of many soils, and moistures less than this value are not readily attained under field conditions. Thus, a simulated radar overpass on Day 35 observes moisture conditions which range between 10 percent and 32 percent of the 1/3-bar water retention in the 0 to 5 cm layer. Such moisture levels are typical of those observed within the data base region during droughts in 1975 and 1976.

The given moisture conditions for the four simulations as described above are tabulated in Table 6. Figure 5 shows an image presentation of the moisture input into the simulations for Case 3 (ten days after the thunderstorm). Roads, buildings, and water bodies are shown in black in this figure and greytone level is proportional to M_{FC} .

SIMULATION PROCEDURE

Figure 6 shows a flow diagram of the simulation procedure used in generating the radar images. The left column contains input information that is either calculated from geometrical considerations or is available in the data base in matrix form. For each cell (pixel), the input information is used to determine the local angle of incidence θ_i through range and slope calculations. This is shown by the top three steps in the right column of Figure 6. The fourth step computes the mean backscattering coefficient, $\bar{\sigma}^\circ$, for that cell. The computation is based on a set of functions that define $\bar{\sigma}^\circ$ as a function of θ_i and the soil moisture content (if applicable) for each of the land use categories given in Table 4. These functions are based on regression

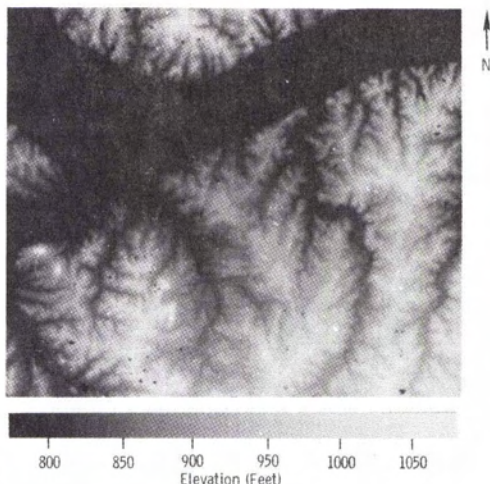


FIG. 4. Elevation map of test site relative to mean sea level.

TABLE 6. VALUES OF RAINFALL AND EVAPORATION USED TO DERIVE THE HYPOTHETICAL SOIL MOISTURE CONDITIONS

Simulation Number, N	Day Number	Rainfall, cm	M_{rain} g/cm ³	Mean Evaporative Rate, cm/day	Number of Elapsed Days	M_{evap} g/cm ³	% of 1/3-bar water content	Estimate M_{FCN}	
								Max.	Min.
1	4	not determined	> > FC	not determined	3	—	$M_{FC1} = 100.0$	100.0	100.0
2	5	≤ 2.5	≤ 0.25	not determined	0	0.0	$M_{FC2} = M_{FC1} + 100(M_{rain}/FC)$ and $M_{FC2} \leq 150.0$	150.0	100.0
3	15	0	0	0.1	10	0.2	$M_{FC3} = M_{FC2} - 20/FC$ and $M_{FC3} \geq 25.0$	90.7	25.0
4	35	0	0	0.005	20	0.2	$M_{FC4} = M_{FC3} - 20/FC$ and $M_{FC4} \geq 10.0$	31.5	10.0

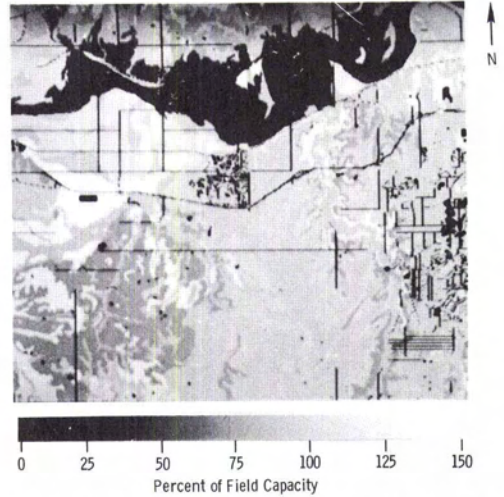
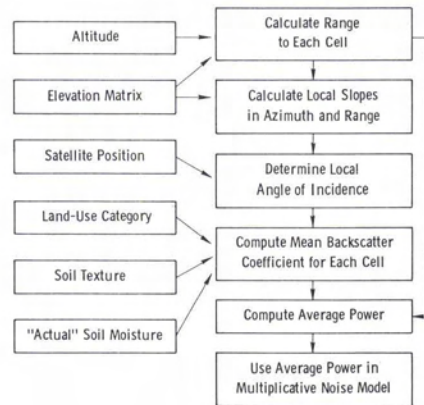


FIG. 5. Actual soil moisture distribution 10 days after the thunderstorm.

fits of experimental data.¹³ For a given value of $\bar{\sigma}^0$, the average power, \bar{P}_r , received by the radar from that cell is computed using the appropriate radar equation.¹³ This power, however, corresponds to the perfectly incoherent case, for which the number of independent samples, N , is infinite. For N finite (see Table 3), Rayleigh fading is involved,¹⁶ in which case the received power, P_r , is a sample from a chi-square (χ^2) distribution with $2N$ degrees of freedom and with mean \bar{P}_r . Generation of P_r for given values of N and \bar{P}_r is accomplished through the use of a random number generator. This value of P_r is then digitized and stored for subsequent use in the interpretation process. For visual display purposes, the digitized value of $10 \log P_r$ is converted into a gray level; Figures 7 to 9



$$P_r = \frac{\bar{P}_r}{2N} \cdot Y \quad Y \sim \chi^2_{2N}$$

FIG. 6. Simulation procedure.

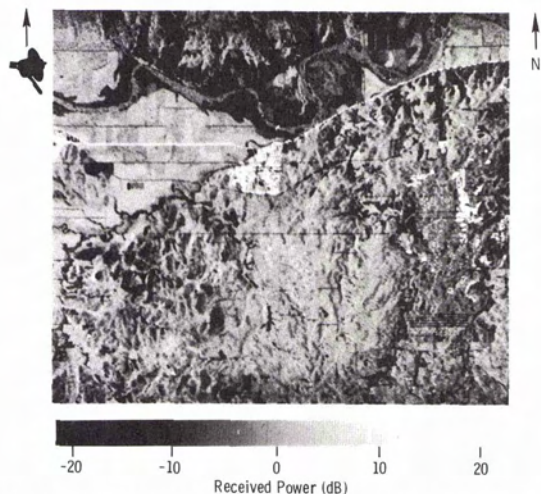


FIG. 7. Simulated radar image for the condition 10 days after the thunderstorm spatial resolution is 20 m by 20 m.

show simulated radar images for the 20 m, 100 m, and 1 km linear resolutions, all for moisture condition 3 of Table 6 (ten days after thunderstorm).

INTERPRETATION PROCEDURE

Whereas the function of the simulation procedure of the last section was to generate a radar image (given detailed information about each cell including local slope, local angle of incidence, land-use category, soil texture, and actual soil moisture content), the function of the interpretation procedure is to generate an "estimated" soil moisture map from the radar image with very lim-

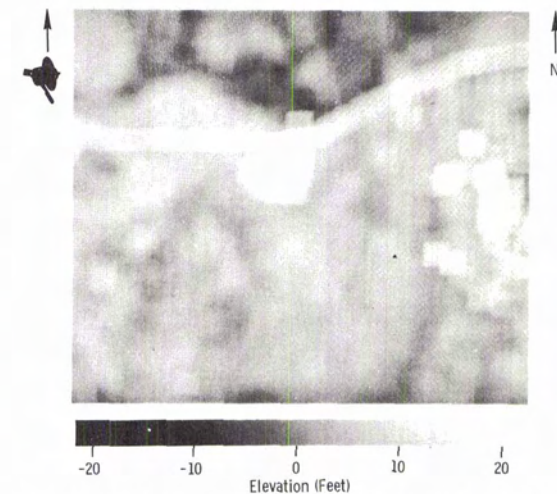


FIG. 9. Simulated radar image for the condition ten days after the thunderstorm spatial resolution is 1 km by 1 km.

ited auxiliary information. Specifically, the only available auxiliary information is the satellite altitude and position relative to a cell and the mean elevation of the scene. From these geometrical parameters, the range to the cell and an assumed angle of incidence, θ , are computed, assuming spherical Earth geometry, constant orbital altitude relative to mean sea-level, and a constant mean elevation of the data base. That is, the value of θ computed for a given cell does not take into account local slope as such information is assumed unavailable in the interpretation process.

From knowledge of the radar system parameters and the range to a given cell, the power, P_r , of that cell is converted to an estimated scattering coefficient value, σ° . Thus, for each cell, the input to the interpretation procedure consists of only σ° and θ for that cell. The soil moisture of that cell is estimated from a general interpretation algorithm given by

$$\hat{M}_{FC} = [\sigma^\circ - f(\theta)]/g(\theta) \quad (6)$$

where

\hat{M}_{FC} = estimated soil moisture of the 0 to 5 cm layer, in percent of field capacity (defined here as the 1/3 bar moisture content);

σ° = scattering coefficient, dB; and

$f(\theta), g(\theta)$ = empirically-determined polynomials (expressions are given in Ulaby *et al.*¹³).

The above algorithm was developed for an amalgamation of all agricultural-scene data acquired by the University of Kansas Soil Moisture Program over the past eight years. The polynomials, $f(\theta)$ and $g(\theta)$, were empirically determined

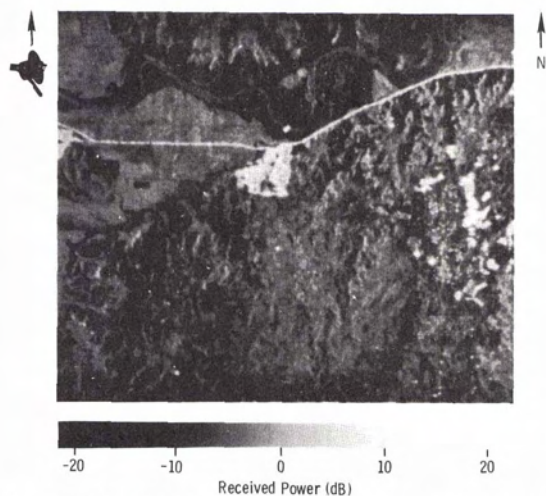


FIG. 8. Simulated radar image for the condition ten days after the thunderstorm spatial resolution is 100 m by 100 m.

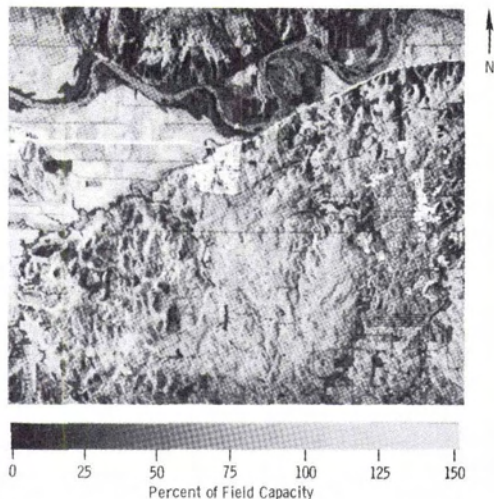


FIG. 10. Predicted soil moisture distribution for the case ten days after the thunderstorm based on 20 m by 20 m radar image.

using 324 data sets, each consisting of σ^0 measurements as a function of θ . These data sets include 181 data sets for bare soil fields covering a wide variety of soil surface roughnesses and soil textural classes, and 143 of vegetation-covered fields covering a wide range of growth stages for wheat, corn, milo, soybeans, alfalfa, and pasture.

Figure 10 shows a predicted soil moisture distribution generated by applying the general soil moisture algorithm to the radar image of Figure 7 (greytone level is linearly related to \hat{M}_{FC}). Of course, this "blind" algorithm is inapplicable to

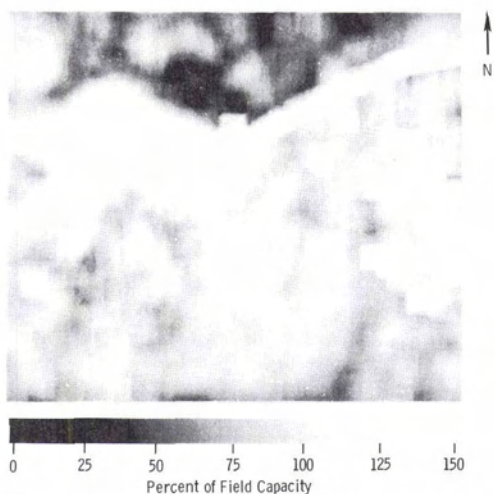


FIG. 11. Predicted soil moisture distribution for the case ten days after the thunderstorm based on 1 km by 1 km radar image.

water surfaces, residential areas, highways, railroads, and trees, and therefore the predicted "moisture" of these classes is meaningless. However, most of these targets are delineated on the predicted soil moisture image, and by matching the image to a map of the scene, most of the non-agricultural cells may be removed from further analysis. This procedure is not possible for the 1 km resolution case shown in Figure 11, except for large features, such as cities and major rivers. On the other hand, as the radar image resolution is made coarser, errors in the predicted soil moisture—due to local slope, surface roughness, and crop-cover variations—are smoothed out, thereby resulting in a better soil moisture estimate. The relations between spatial resolution and soil moisture estimation accuracy are examined in the next section.

EVALUATION OF MOISTURE ESTIMATION ACCURACY

Precise evaluation of the accuracy of the estimated (predicted) moisture was complicated by the geometric relief displacements inherent in the radar imaging process. While the relatively small vertical relief of the data base produced insignificant layover and shadowing in the resultant images, foreshortening produced a geometric displacement of upland surfaces by as much as 100 metres relative to the surface defined by the river floodplain.

Quantitative evaluation of moisture estimate accuracy by machine assumes that the radar image can be accurately mapped back into the coordinate system defined by the original data base. Because of the complexity of image rectification to account for range creep caused by foreshortening in the radar images, a dual approach was followed to establish estimate accuracy. In the first and "worst-case" approach, moisture estimate error is examined for the entire data base and includes errors associated with imaging geometry problems and the effects of unknown local slope. In the second approach, moisture estimate accuracy will be considered only for the relatively flat region of the river floodplains where elevation of the data base is less than or equal to 820 feet. Both analytic approaches utilized a common set of moisture-estimate-error maps.

Furthermore, regardless of approach, estimate accuracy was evaluated by comparing estimated moisture \hat{M}_{FC} to the input "actual" moisture M_{FC} existent within the central 20 m by 20 m area of the resolution cell. In effect, all three radar system resolutions were used to estimate soil moisture at a 20 metre resolution and then compared to the input soil moisture at a 20 metre resolution. Thus, this procedure offered a very stringent test of estimate accuracy for the coarse resolution radar systems.

Estimate error maps were produced by the fol-

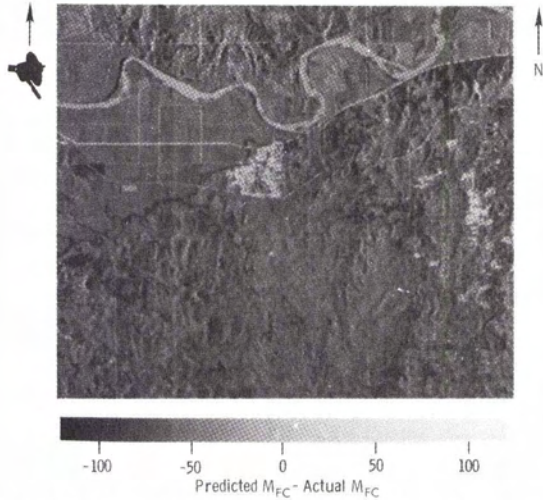


FIG. 12. Magnitude of (predicted-actual) soil moisture for the condition ten days after the thunderstorm based on the 20 m by 20 m radar image.

lowing procedure. A set of five control points was identified on the simulated radar imagery for recognizable features on the floodplain. These same features were located on the data base. The mean distance between the control points as identified on the radar imagery and those on the data base was used to translate the coordinate system of the estimated moisture image. The estimated moisture image was not rotated or warped. The resultant estimated moisture matrix was then compared to the "actual" moisture matrix from the data base with a registration error of ± 20 metres on the floodplain and ± 100 metres on the upland surfaces due to uncorrected range creep. Thus, for a given resolution and moisture condition, the estimated moisture \hat{M}_{FC} and "actual" moisture M_{FC} could be compared on a pixel by pixel basis relative to the 20 m by 20 m resolution cells of the data base.

Figure 12 shows the difference between estimated and actual moisture for moisture condition 3 (ten days after the thunderstorm) based on the 20 m resolution radar image. The image graytone G_E (between 0 and 255) of the ij pixel element is defined as:

$$G_{Eij} = \hat{M}_{FCij} - M_{FCij} + 128 \quad (7)$$

Thus, for a given image, $G_E = 128$ (medium gray) represents zero difference between estimated and actual moisture, bright pixel elements with $G_E \gg 128$ represent large overestimates of moisture, and dark pixel elements with $G_E \ll 128$ correspond to large underestimates of "actual" moisture.

For any of the three simulated resolutions, some general observations can be made regarding esti-

mate error as a function of certain data base characteristics.

Pixels with zero moisture in the data base. By definition, all target classes in the data base for which "actual" moisture is undefined and arbitrarily set to zero will result in large moisture estimate errors. Bridges, buildings, and railroads will always produce a moisture estimate \gg zero. For water bodies and roads, "actual" moisture is undefined and set equal to zero, while estimated moisture for these target classes is always greater than zero. Thus, such targets are generally bright on the error map (Figure 12). These targets comprise 7.4 percent of the data base.

Tree canopies. Tree canopies are assumed to completely attenuate the backscatter contribution from the underlying soil at the simulated frequency. Thus, estimated moisture is generally far less than "actual" moisture except for the very dry conditions simulated for moisture condition 4 (30 days after the thunderstorm). Deciduous trees comprise 13.0 percent of the data base.

Local slope effects. Since Equation 6 is a blind classifier of the radar image, a predictable error component is introduced into the error maps because of the high sensitivity of σ° to θ_i near nadir. In general, moisture is overestimated for west-facing local slopes (those toward the satellite) while moisture is underestimated for east-facing local slopes (those away from the satellite). As would be expected, these effects are most noticeable for the dissected upland areas to the north and south of the river floodplain, particularly for the 20-metre resolution. Coarser resolution tends to average many of these errors associated with the effects of local slope.

Range creep. The translation of features on the radar imagery relative to the data base as a function of elevation by foreshortening produces a double error component on the error maps. Since radar-image-to-data-base rectification was performed to minimize position errors on the floodplain, this error component is most noticeable in the dissected upland region in the lower right side of the error maps. Moisture estimate errors in this region resemble "ghost images," especially for linear features such as roads. The "ghost" errors are approximately equal in magnitude but opposite in sign and are separated by one to five pixel elements on the 20 m resolution image depending upon local elevation. These double estimate errors are artifacts of the comparison methodology and relate to the position of a feature such as a road on the data base and its offset location on the interpreted radar imagery.

ESTIMATION ACCURACY OVER THE TOTAL DATA BASE

An example of the relationship between absolute estimate error and cumulative percent of the 800,000 pixels in the total base is presented in

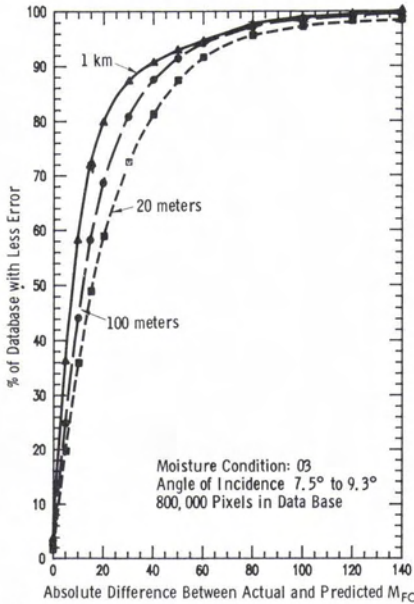


FIG. 13. Soil moisture estimate accuracy for the entire simulation data base with moisture condition 3, ten days after thunderstorm, and at angles of incidence between 7.5° and 9.3°. Absolute difference is computed at a 20 metre resolution.

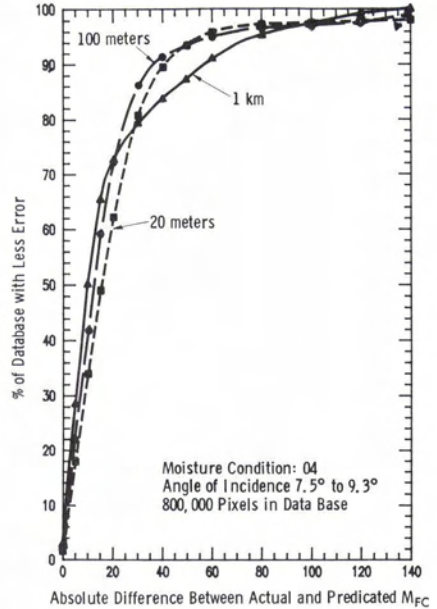


FIG. 14. Soil moisture estimate accuracy for the entire simulation data base with moisture condition 4, drought, and at angles of incidence between 7.5° and 9.3°. Absolute difference is computed at a 20 metre resolution.

Figure 13 for moisture condition 3. The relationship between absolute estimate error and gravimetric moisture is given in Table 7 for loamy sand, silt loam, and silty clay loam. The results in Figure 13 represent a "worst case" evaluation of moisture estimation accuracy because no adjustment is made to account for errors caused by geometric registration problems, the effects of local slope, or the inclusion of data base categories where moisture is undefined. It should also be remembered that all radar resolutions are used to estimate moisture at a 20 metre resolution. The trend toward increasing estimate accuracy at coarser resolutions also was observed for simula-

tion moisture conditions 1 and 2 (Table 6). This result is apparently due to several considerations:

- "Actual" moisture does not vary dramatically between adjacent 20 m by 20 m data base pixels, except at the boundaries of soil types;
- the coarser resolutions average the local effects of slope, canopy cover type, row direction, and surface roughness; and
- the effects of water bodies, cultural targets, and forested areas are averaged over much larger areas.

For moisture condition 4, drought conditions, the accuracy of the 1 km resolution is poorer than that provided by the finer resolutions as shown in Figure 14. This is caused by the effects of cultural targets; categories such as buildings, bridges, and railroads have a $\bar{\sigma}^\circ$ of 10 dB and for very dry moisture conditions, $\bar{\sigma}^\circ$ of agricultural targets is typically 20 to 25 dB less. Thus, during extremely dry conditions, the large spatial averaging inherent in the 1-km resolution will cause a significant over-estimation in the moisture present in agricultural scenes adjacent to cultural targets with very large $\bar{\sigma}^\circ$. As a consequence, it is expected that the spatial density of such targets within a given area will effectively determine the upper limit of desirable resolution for sensing very dry soil moisture conditions. Thus, for agronomic regions similar to the data base, resolutions on the order of 1 km would be adequate for dry conditions, while for areas

TABLE 7. ESTIMATE ACCURACY LEVELS: COMPARISON OF ABSOLUTE ERROR IN PERCENT OF FIELD CAPACITY TO PERCENT GRAVIMETRIC MOISTURE FOR LOAMY SAND, SILT LOAM, AND SILTY CLAY LOAM

Field Capacity Accuracy Level	Gravimetric Moisture		
	± Estimate Accuracy in Percent		
	Loamy Sand	Silt Loam	Silty Clay Loam
10%	0.9	2.4	3.1
20%	1.8	4.8	6.2
30%	2.7	7.3	9.2

TABLE 8. CUMULATIVE PERCENT OF AGRICULTURAL FLOODPLAIN WITHIN CERTAIN ABSOLUTE ERROR LIMITS FOR C-BAND SIMULATION RESULTS AT $\theta = 7.5^\circ-9.3^\circ$

Approx. User Accuracy Level \rightarrow +/- % of field capacity \rightarrow		1	2	3	4	5
		50	40	30	20	10
Moisture Condition \downarrow	Resolution \downarrow					
1	20 \times 20 m	96.4	94.3	89.9	79.1	52.4
	93 \times 100 m	99.6	98.7	96.2	87.6	63.8
	1 \times 1 km	100.0	99.9	99.4	96.3	76.8
2	20 \times 20 m	93.6	88.5	79.2	64.4	39.6
	93 \times 100 m	98.9	95.7	87.6	75.4	47.2
	1 \times 1 km	100.0	99.9	98.8	92.8	68.7
3	20 \times 20 m	97.1	95.3	91.3	80.9	53.2
	93 \times 100 m	98.9	98.0	96.0	89.2	64.0
	1 \times 1 km	99.0	98.2	94.6	85.9	60.6
4	20 \times 20 m	97.9	95.9	89.8	71.4	39.7
	93 \times 100 m	97.2	96.2	93.6	81.2	47.4
	1 \times 1 km	89.0	84.4	82.7	77.6	50.5

All pixels in the data base where elevation is >820 feet are excluded and all non-agricultural pixels are excluded from analysis. All radar resolutions are used to estimate moisture at a 20 metre ground resolution.

such as the high plains (where the density of cultural targets is lower than that simulated) resolution >1 km might prove adequate. On the other hand, accurate sensing of dry moisture conditions in regions with dense distributions of hard cultural targets, such as the northeastern United States and northern Europe, would require a resolution less than 1 km.

ESTIMATION ACCURACY WITHIN THE FLOODPLAIN

In order to minimize the analytic bias introduced by uncorrected foreshortening of the predicted moisture maps, moisture estimate accuracy is presented in Table 8 for each resolution and moisture condition for only those pixels on the relatively flat river floodplain. Approximately 183,000 pixels comprise this region, or about 23 percent of the data base. Geometric registration of the predicted moisture maps to the coordinate grid of the data base was optimized for this region. The floodplain was arbitrarily defined by all pixels in the data base with elevation less than or equal to 820 feet. In addition, the values given in Table 8 exclude pixels classified in the data base as water bodies, buildings, railroads, bridges, roads, trees, and sandbars, thus minimizing the estimate error component related to undefined or unsensible "actual" soil moisture.

The 1 km resolution results in the highest estimate accuracy at all accuracy levels except for the very dry moisture condition that corresponds to 30 days after the thunderstorm. Also, estimate accuracy is generally lower at all resolutions for either the extremely wet or extremely dry moisture con-

ditions (moisture conditions 2 and 4, respectively) than for the more typical intermediate moisture conditions. This is expected since the effects of surface roughness and crop canopy cover cause a divergence of $\bar{\sigma}^\circ$ between target classes at the moisture extremes.

The cumulative percent of the 183,000 pixels comprising the agricultural floodplain is plotted versus maximum absolute estimate error in Figure 15 for moisture condition 3. Similar results were obtained for moisture conditions 1 and 2, but for the drought case (condition 4), the accuracy of the 1 km resolution is lower than that of the 100 metre resolution (see Table 8). This is again caused by the averaging of relatively high $\bar{\sigma}^\circ$ from cultural targets, which, for the simulated floodplain region, is primarily related to the presence of a railroad running east to west and secondarily to scattered point-targets such as buildings.

Recent efforts to identify the user requirements for a soil moisture sensing system have produced the accuracy, resolution, and repeat coverage requirements shown in Tables 9 and 10.¹⁸ For most of the surveyed uses, resolutions greater than or equal to 100 metres with repeat coverage from three to seven days are acceptable. Most uses specified moisture estimate accuracies between 3 and 5 which are approximately ± 30 percent of M_{FC} and ± 10 percent of M_{FC} , respectively, from Table 11. For the simulated moisture conditions, accuracy level 3 is achieved for over 90 percent of the 20 metre pixels on the river floodplain even from 100 metre and 1 km resolution imagery. Additionally, these results are significantly improved

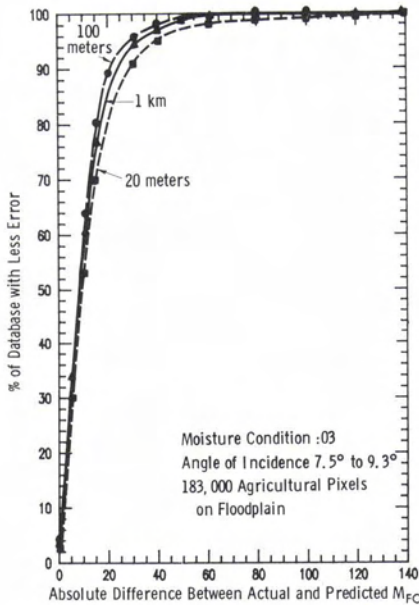


FIG. 15. Soil moisture estimate accuracy for agricultural categories on the floodplain with moisture condition 3, ten days after thunderstorm, and at angles of incidence between 7.5° and 9.3°. Absolute difference is computed at a 20 metre resolution.

when estimated moisture \hat{M}_{FC} is compared to the mean moisture over the full nominal area of the resolution cell, instead of the one 20 metre pixel at the center of the resolution cell. As an example, for moisture condition 2 at user accuracy level 5, Table 8 shows the 1 km radar resolution results in a correct moisture classification of 68.7 percent of the area at a 20 metre resolution; however, 82.1 percent of the area is correctly classified when the

1 km radar resolution is used to estimate moisture at a 1 km resolution.

CONCLUSIONS

The validity of the results derived from any simulation of a real-world situation is inherently limited by the degree of realism incorporated in the assumptions and models used in generating the simulations. In the present study, the aspect of realism is governed by three types of factors: (a) geometrical factors associated with the image formation process of a sidelooking imaging radar, (b) signal fluctuations due to Rayleigh fading (speckle effect) in radar images that contain a small number of independent samples per pixel element, and (c) the models characterizing the backscatter behavior of the various target classes contained in the simulated scene. The first two types of factors are well understood; therefore, it was possible to incorporate them in the simulation algorithm with a high degree of accuracy. This accuracy was verified in a separate study through comparisons of simulated SAR images with actual images of the same scene.¹⁷ The degree of realism associated with the third type of factor—the backscatter models—is very good, if considered in statistical terms. That is, the functions used to describe the dependence of the backscattering coefficient $\bar{\sigma}^\circ$ on the local angle of incidence θ_i and moisture content M_{FC} (for agricultural categories) are based on statistical regressions applied to experimental data obtained over the past eight years. In the majority of cases, the correlation coefficients associated with these regressions are greater than 0.8, which means that the regressions account for the majority of the observed variation in $\bar{\sigma}^\circ$, but some variation, part of which is due to measurement error, remains unaccounted for. Considering that the overall study is, to some extent, statistical in nature, the

TABLE 9. SOIL MOISTURE INFORMATION AND DATA REQUIREMENTS AT DIFFERENT CROP PRODUCTION STAGES (FROM SOIL MOISTURE WORKING GROUP¹⁸)

Crop Production Stage	Accuracy Level*	Frequency (Days)	Resolution (km ²)	Depth
Planning (Acreage & Yield Predictions)	3-5	7-20	1-15	profile
Ground Preparation & Planting	1-3	5	0.5-1	surface layer
Germination	3	5	1-10	surface layer
Growth & Development				
Nutrient Supply	3	7-10	1-10	profile
Water Management-Irrigation	5	3	0.5	profile
Water Management-Drainage	3	3-5	1-10	profile
Pest Management	5	3	0.5	surface layer
Maturing-Yield Estimate	3-5	3-10	0.5-1	profile
Harvest	3	3-7	0.5	surface layer

* 1 = General accuracy of High, Medium, or Low
 2-4 = Gradation between Accuracy Levels 1 and 5
 5 = +/- 4% accuracy by value measurement

TABLE 10. SOIL MOISTURE INFORMATION AND DATA REQUIREMENTS IN HYDROLOGY (FROM SOIL MOISTURE WORKING GROUP¹⁸)

Soil Moisture Applications and Identified Users	Accuracy Level*	Frequency (Days)	Resolution (km ²)
<i>Runoff Potential:</i>			
Federal Users: NOAA-NWS, USACE, SCS Design Engineers WPRS, HUD Flood Insurance Program State Users: Highway Departments & Water Resource Centers County and City Governments Private Power Companies	1**	3-7	5-25
<i>Erosion Losses:</i>			
Federal Users: Design Departments of USACE, USDI, and USDA-SCS	3	3	5-25
County Organizations of Governments	5	3	0.5
Farmers' Organizations	3	3	1
<i>Reservoir Management:</i>			
Federal Users: USACE, WPRS	1	3-7	5-25
State and Local Users: Water Resource Centers	3	3-7	0.5
Private Power Companies, Regional Planners, Recreation Industries	3	3-7	0.5
<i>Infiltration for Trafficability and Structure Design</i>			
Federal Users: USACE, USDA-SCS	5	3	0.5
State Users: Drainage Districts, Planners	5	3	0.5
Private Irrigation Design Engineers, Mining Engineers, Developers	5	3	0.1
<i>Water Quality</i>			
Pesticide and Nutrient Losses:			
Federal Users: EPA, FDA, USDA-SCS	5	3	0.1
State Users: Water Resource Centers	3-5	3	0.1-0.5
Private Irrigators, Farm Organizations, Feed-Lot Operators, Hydrologic Engineers, Planners & Developers	1-3	3-7	5

*1 = General accuracy of High, Medium, or Low

2-4 = Gradation between Levels 1 and 5

5 = ±2% accuracy by volume measurement.

** = Data refer only to the users on the respective line in the table.

approach used above for modeling the backscatter behavior is certainly justified.

The major conclusions derived from this study are

(1) Among the three radar resolutions considered (20 m, 100 m, and 1 km), soil moisture content was estimated at a 20 metre resolution with the highest accuracy by the 1 km resolution radar images for the relatively wet soil conditions (Cases 1

and 2 of Table 6), comparable levels of accuracy were provided by the 100 m and 1 km resolutions for Case 3 (ten days after the thunderstorm), and the 100 m resolution provided significantly better results than the 1 km resolution for the drought case (30 days after the thunderstorm). Within the context of the simulated conditions, the superiority of the coarse resolutions in estimating soil moisture is explained by the capacity of the coarse resolutions to function as low pass spatial filters where high spatial frequency noise is related to signal fading, land-use category, surface roughness, row direction, and local slope.

(2) Based on the above results, it appears that a spatial resolution between 100 m and 1 km would provide optimum performance over the various soil moisture conditions. Narrowing this range down to a specific value is the object of a further phase of this investigation and is certainly dependent upon the spatial distribution of soil moisture and other scene elements.

(3) This study was performed for a test site in eastern Kansas, where dry-land farming practices

TABLE 11. APPROXIMATE RELATIONSHIP BETWEEN UNCERTAINTY IN PERCENT OF FIELD CAPACITY AND USER REQUIREMENTS OF MOISTURE ESTIMATE ACCURACY

User-Defined Accuracy Level ¹⁴	Uncertainty in % of Field Capacity
1	+/- 50%
2	+/- 40%
3	+/- 30%
4	+/- 20%
5	+/- 10%

prevail. For such regions, the periodic structure associated with soil surfaces of row crops exercises a minor influence on the scattering behavior as a function of radar look-direction relative to row-direction (for the sensor parameters specified in this study). In regions where irrigation practices are common, the row structures usually have larger amplitudes, which would lead to greater ambiguity in the soil moisture estimation process for like-polarized radar configurations. Research conducted to date indicates that the cross-polarized scattering coefficient is significantly less sensitive to row direction and, therefore, should be preferred for mapping soil moisture content in irrigated regions. The major drawback to the use of cross-polarization is the fact that more transmitter power is required than for the like-polarized case. However, since the needed resolution is on the order of hundreds of metres, it may be possible to configure a cross-polarized space radar system with existing technology.

REFERENCES

1. Ulaby, F. T., and P. P. Batlivala, Optimum Radar Parameters for Mapping Soil Moisture, *IEEE Transactions on Geoscience Electronics*, Vol. GE-14, No. 2, pp. 81-93, April 1976.
2. Ulaby, F. T., P. P. Batlivala, and M. C. Dobson, Microwave Backscatter Dependence on Surface Roughness, Soil Moisture and Soil Texture: Part I—Bare Soil, *IEEE Transactions on Geoscience Electronics*, Vol. GE-16, No. 4, pp. 286-295, October 1978.
3. Ulaby, F. G., G. A. Bradley, and M. C. Dobson, Microwave Backscatter Dependence on Surface Roughness, Soil Moisture and Soil Texture: Part II—Vegetation-Covered Soil, *IEEE Transactions on Geoscience Electronics*, Vol. GE-17, No. 2, pp. 33-40, April 1979.
4. Dobson, M. C., and F. T. Ulaby, Microwave Backscatter Dependence on Surface Roughness, Soil Moisture and Soil Texture: Part III—Soil Tension, *IEEE Transactions on Geoscience and Remote Sensing*, Vol. GE-19, No. 1, pp. 51-61, January 1981.
5. de Loor, G. P., Soil Moisture Determination at X-Band, *Proceedings of the Microwave Remote Sensing on Bare Soil Workshop*, EARSeL, Paris, pp. 198-202, April 1979.
6. Haruto, Hirosawa, S. Komiyama, and Y. Matsuzaka, Cross-Polarized Radar Backscatter from Moist Soil, *Remote Sensing of Environment*, Vol. 7, No. 3, pp. 211-217, August 1978.
7. Ulaby, F. T., and J. E. Bare, Look Direction Modulation Function of the Radar Backscattering Coefficient of Agricultural Fields, *Photogrammetric Engineering and Remote Sensing*, Vol. 45, No. 11, pp. 1495-1506, November 1979.
8. Bradley, G. A., and F. T. Ulaby, *Aircraft Radar Response to Soil Moisture*, RSL Technical Report 460-2 (AGRISTARS SM-KO-04005), University of Kansas Center for Research, Inc., Lawrence, Kansas 66045, October 1980.
9. Fenner, R. G., G. F. Pels, and S. C. Reid, *A Parametric Study of Tillage Effects on Radar Backscatter*, Terrain and Sea Scatter Workshops Report, Washington, D.C., (printed by Remote Sensing Laboratory, University of Kansas, Lawrence, Kansas 66045), March 1980.
10. Le Toan, T., G. Flouzat, M. Pausader, A. Fluhr, and A. Lopes, *Multifrequency Radar Measurements of Soil Parameters*, COSPAR, Budapest, Hungary, June 1980.
11. Ulaby, F. T., M. Dobson, and G. Bradley, *Radar Reflectivity of Bare and Vegetation-Covered Soil*, COSPAR, Budapest, Hungary, June 1980.
12. Jackson, T. J., A. Chang, and T. J. Schmugge, Aircraft Active Microwave Measurements for Estimating Soil Moisture, submitted for publication in *Photogrammetric Engineering and Remote Sensing*.
13. Ulaby, F. T., C. Dobson, J. Stiles, R. K. Moore, and J. Holtzman, *Evaluation of the Soil Moisture Prediction Accuracy of a Space Radar Using Simulation Techniques*, RSL Technical Report 429-1, University of Kansas Center for Research, Inc., Lawrence, Kansas 66045, March 1981.
14. Moore, R. K., Tradeoff Between Picture Element Dimensions and Noncoherent Averaging in Side-Looking Airborne Radar, *IEEE Transactions on Aerospace and Electronic Systems*, Vol. AES-15, No. 5, pp. 697-708, 1979.
15. Schmugge, T. J., Effect of Texture on Microwave Emission from Soils, *IEEE Transactions on Geoscience and Remote Sensing*, Vol. GE-18, No. 4, pp. 353-361, October 1980.
16. Bush, T. F., and F. T. Ulaby, Fading Characteristics of Panchromatic Radar Backscatter from Selected Agricultural Targets, *IEEE Transactions in Geoscience Electronics*, Vol. GE-13, No. 4, pp. 149-157, October 1975.
17. Stiles, J. A., V. S. Frost, S. A. Smith, and J. C. Holtzman, *Coherent and Partially Coherent Radar System Models and Simulation*, RSL Technical Report 418-1, University of Kansas Center for Research, Inc., Lawrence, Kansas 66045, October 1980.
18. Soil Moisture Working Group, *Plan of Research for Integrated Soil Moisture Studies*, Recommendations of the Soil Moisture Working Group, NASA/GSFC, October 1980.

(Received 4 May 1981; revised and accepted 16 October 1981)